Synthesis of polyimide-modified carbon nanotubes as catalyst for organic pollutant degradation via production of singlet oxygen with peroxymonosulfate without light irradiation

Mingyu Wei[a,b], Xiaowen Shi[a], Ling Xiao*[a], Haifei Zhang*[b]

[a] *School of Resource and Environmental Science, Key Laboratory for Biomass-Resource Chemistry and Environmental Biotechnology of Hubei Province, Wuhan University, Wuhan 430072, PR China*

[b] *Department of Chemistry, University of Liverpool, Liverpool L69 7ZD, United Kingdom*

* Corresponding author.

xiaoling9119@whu.edu.cn (L. Xiao), Fax: +86 2768763162, Tel: +86 2768778652.

zhanghf@liverpool.ac.uk (H. Zhang), Fax: +44 151 7943588, Tel: +44 151 7943545

Abstract

Polyimide-modified carbon nanotubes (PI/CNTs) were synthesized via a solvent-free thermal method and used as a metal-free catalyst to activate peroxymonosulfate for organic contaminant degradation without light irradiation. The characterization results suggested that PI was loaded onto the surface of CNTs. The catalytic ability of the PI/CNTs was strongly correlated with the content of PI in the catalysts. The PI/CNTs (22% of PI) showed the highest catalytic efficiency for organic pollutant degradation at room temperature. The degradation efficiency of acid orange 7 (AO7) dye was significantly enhanced to 98.9% within 15 min, compared to the efficiency of 2.2% exhibited by pure PI. The radical quenching tests and electron paramagnetic resonance spectrometry proved that singlet oxygen, instead of hydroxyl radicals or sulfate radicals, played a dominant role during the catalytic oxidation of AO7. The influences of operation parameters including temperature and catalyst amount were investigated. The PI/CNTs metal-free catalyst exhibited high catalytic activity under a broad range of pH values. The recycling study of four repeated reactions demonstrated good stability of the PI/CNTs. This work provided a promising metal-free catalyst for degradation of organic pollutants in aqueous solutions, contributing to the development of green materials for sustainable remediation.

Keywords: Polyimide; Carbon nanotubes; Organic pollutants; Peroxymonosulfate; Photodegradation

1. Introduction

With the development of society, the wastewater discharged from industrial processes has become a serious environmental problem due to their recalcitrance and toxicity to animals and human beings [1]. In recent decades, advanced oxidation processes (AOPs) including photocatalysis [2], ozonation [3], electrochemical treatment [4], Fenton and Fenton-like processes [5] have provided important and efficient solutions in the degradation of organic pollutants (i.e., dyes). Much attention has been paid to persulfates (i.e., peroxymonosulfate (PMS) and peroxydisulfate (PDS)) based on advanced oxidation technologies [6], owing to its strong oxidation characteristics and high chemical stability. The reactive oxidized species (i.e., HO•, SO_4^{-}•,$^1O_2$) could be generated via activation of the persulfates by using heat, UV and transition metal ions [7-10]. The photocatalytic capacity may be further improved with the use of hierarchical nanostructures under irradiation of visible light [11].Thermal activation is required by heating the solution, which is costly and presents many engineering challenges [12]. Additional cost may be incurred because the liquid needs to be pumped out before treatment under UV light [13]. Transition metal ions (i.e., Cu^{2+}, Co^{2+}, Mn^{2+}, Ru^{3+}, V^{3+}, Ce^{3+} and Ni^{2+}) accompanied with PMS show efficient degradation of organic pollutants [14,15], but these metal ions catalysts can cause potential health problems and may be difficult for recycling. In the past two decades, many researchers have shifted their focus from the homogeneous system to the heterogeneous system where catalysts may be easily recycled and there may be no need

to deal with secondary pollution [16]. Thus, the metal-free materials, without the problem of metal ions leaching, have gradually become the preferred choice as heterogeneous catalysts for persulfate activation.

Metal-free carbonaceous materials such as activated carbon (AC), graphene, reduced graphene oxide (rGO), and carbon nanotubes (CNTs) can be used as heterogeneous catalysts with advantages including no metal ions leaching, high chemical stability, and environmental friendliness. CNTs have attracted great interests due to their unique structure, excellent electronic and mechanical properties. As reported recently, CNTs were used as persulfate activators to degrade the organic pollutants through radical and non-radical mechanisms. Sun, *et al*. reported that CNTs could activate PMS and PDS to generate sulfate radicals for the degradation of phenol [17]. Lee, *et al*. found that persulfates could be activated by CNTs via a non-radical mechanism, forming reactive species which were capable of effectively degrading organic pollutants [18]. The catalytic efficiency of CNTs-activated PMS could be improved considerably through modification of CNTs. For example, N-doped CNTs were shown to give enhanced catalytic performance after modifying the intrinsic structure of CNTs [19]. It was proposed that N-doped carbon materials gave a better balance between graphitization degree and surface graphitic nitrogen sites, which led to the conclusion that non-radical pathways ($^1O_2$) played a vital role in the degradation of bisphenol A. However, the catalytic efficiency of such catalysts is still very low and hence novel metal-free catalysts which can activate PMS with low cost and high

catalytic performance are highly sought after.

Polyimides (PI) have many excellent properties such as high glass transition temperature, excellent electrical, mechanical & thermal stability, and high chemical resistance. Polyimides and their derivatives have therefore been successfully used in many industrial applications [20,21]. Recently, the photocatalytic activity of PI has attracted attention for its promising potential applications in generating H_2 from water [22] and degrading organic pollutants [23]. The metal-containing organic–inorganic composite of PI showed good photocatalytic performance for the degradation of rhodamine B (RhB) and methyl orange (MO) under light irradiation [24]. Li, *et al*. [25] found that the inorganic–organic hybrid ZnO-polyimide core-shell hybrids prominently enhanced the degradation of methylene blue (MB) under light irradiation. It was found that S-doped PIs could extend the light absorption range and result in an enhanced photocatalytic activity [26]. The electronegative N atoms have high affinity to organic pollutants while the positively polarized carbon atoms facilitate the adsorption of negatively charged PMS. The enhanced adsorption of pollutants and PMS onto the catalysts promotes the contact between the pollutants and the reactive oxidized species generated from the activation of persulfates, leading to high catalytic activity. PI molecules possess abundant electronegative N and O atoms and positively polarized carbon atoms. Loading of PI molecules on the CNTs can couple the excellent electronic migration and mechanical properties of CNTs with high adsorption ability of PI to produce catalysts with high performance.

In this work, polyimide-modified carbon nanotubes (PI/CNTs) were prepared and used as catalysts for the degradation of organic dyes by activating PMS. It is worth noting that the fabricated materials showed high efficiency in degrading the organic pollutants without light irradiation. The catalytic efficiency of such catalysts was significantly influenced by the loading content of PI on CNTs. It was found that singlet oxygen ($^1O_2$), rather than hydroxyl radical (HO•) and sulfate radical (SO_4^-•), played a dominant role in photodegradation. This work provides an insightful perspective on PMS activation mechanism with metal-free catalysts for oxidation reactions.

2. Experimental

2.1. Materials

CNTs (outside diameter:10-20 nm; length:10-30 μm) was purchased from XFNANO Materials Tech Co. Ltd. Melamine (MA), dicyandiamide (DCD), pyromellitic dianhydride (PMDA), methyl orange (MO), rhodamine B (RhB), Reactive Brilliant Blue KN-R (KN-R), methylene blue (MB), and Reactive Brilliant Red X-3B (X-3B) were purchased from Sinopharm Chemical Reagent Co. Ltd. (Shanghai, China). Acid Orange 7 (AO7) was purchased from Sigma-Aldrich. Oxone ($2KHSO_5 \cdot KHSO_4 \cdot K_2SO_4$), Tert-butanol (TBA), 2,2,6,6-tetramethy l-4-piperidinol (TMP), 5,5-dimethyl-1-pyrroline N-oxide (DMPO), ethanol, were obtained from Aladdin Industrial Inc. All chemicals were used without further purification.

2.2. Preparation of PI/CNTs catalyst

The PI/CNTs catalysts were synthesized by a solvent-free method similar to the procedure for pure PI as described in the literature [27] (Fig S1). In a typical reaction, 2.52 g MA, 4.36g PMDA and 24 g CNTs powders were mixed in an agitating mortar for 30 min. Then, the mixture was put into a quartz boat with a cover in a tube furnace and heated to 325 ^{o}C at a heating rate of 7 ^{o}C/min and maintained for 4 h. The resulting solid was ground to powder and washed with deionized water, and finally dried at 60 ^{o}C overnight. The PI/CNTs (X) catalysts with different mass ratios of PI:CNTs were prepared, with the ratios being 82%, 71%, 43%, 22%, 16%.

2.3. Characterization

Powder x-ray diffraction (PXRD) patterns were obtained on a Bruker D8 Advance X-ray diffractometer for crystalline phase identification. Fourier-transform infrared spectroscopy (FT-IR) analysis was performed on a Bruker Vector 22 spectrometer. N_2 adsorption/desorption isotherms were obtained on a Belsorp-mini II (Japan) at 77 K and a relative pressure (P/P_0) range of 0.005-0.99. Before N_2 sorption analysis, all the samples were thermally treated at 120 ^{o}C for 16 h and then degassed at 120 ^{o}C on the sorption instrument for 3 h. The size and morphology of the catalysts were examined on a Nova 450 scanning electron microscope (SEM), a JEM-2100 transmission electron microscope (TEM) and a Titan (G260-300) high resolution transmission electron microscope (HRTEM) with an accelerating voltage of 300 kV. Energy-dispersive X-ray (EDX) elemental mapping was performed using High-Angle Annular Dark Field-STEM (HAADF-STEM) by Titan G260-300. The C, N and O species were studied by

X-ray photoelectron spectroscopy (XPS) on an ESCALAB 250Xi spectrometer (Thermo Fisher) with an Al K Alpha (1486.6 eV) X-ray source. The samples were measured under an ultrahigh vacuum (SAC $5.0x10^{-10}$ mbar) under the conditions of pass energy (100 eV), beam voltage (15kv, power 150W), and beam size (500 μm). All the high resolution spectra were obtained under CAE mode with pass energy of 30 eV. The deconvolution of N 1s and O 1s XPS spectra was performed using the software with the ESCALAB 250Xi spectrometer (Thermo Fisher) by the Analysis and Testing Centre of Wuhan University. Ultraviolet-visible (UV-vis) spectra were recorded using a UV-2700 spectrophotometer (Shimadzu, Japan). The intermediates were studied by an Esquire LC-ion trap mass spectrometer with an orthogonal geometry ESI source (Bruker Daltonics, Germany). The reactive radical spectra were recorded by the electron paramagnetic resonance spectrometer (EPR, Bruker A300). The visible-light source used was a 300 W Xenon lamp with a 400 nm cutoff filter. The pH was measured using a Leici PHS-3C pH meter (Shanghai, China).

2.4 Organic pollutant degradation

Degradation reactions were carried out in a 100 mL glass reactor with magnetic stirring at 25 ^{o}C. These reactions were performed under indoor normal light unless specified otherwise (for the study on the effect of light irradiation). Typically, 5 mg PI/CNTs (X) was added into 50 mL of 50 mg/L AO7 solution and stirred for 30 min to achieve adsorption equilibrium. The reactions were then started with the addition of the PMS (0.2 g/L). The solution samples were taken at given time intervals and filtered to

remove the catalyst with a membrane (pore size 0.22 μm). H_2SO_4 (10 mM) and NaOH (10 mM) were used to adjust the solution pH to the required values. Buffer solutions with suitable pH were not used in the current study because it was envisaged that the use of buffer solution to control pH could influence the reaction mechanism and complicate the data interpretation. The catalyst in the recycling study was removed from the reaction solution after each test and added into fresh PMS and dye solution for the next test. The concentrations of the pollutant were determined by using a UV-2700 spectrophotometer with a calibration curve.

To investigate the effect of light irradiation, the degradation reactions were performed under the same condition in darkness, exposed under sunlight, or exposed under visible light (a 300W Xenon lamp with a 400 nm cutoff filter, which was 15 cm above the solution surface; a water recycling equipment was used to keep the temperature constant at 25 ^oC).

3. Results and discussion

3.1 Characterization of PI/CNTs

The morphology of the as-prepared materials was observed by HRTEM and SEM, and the images are shown in Fig.1. The CNTs have the diameters around 10 nm (Fig. 1(A)) and show a twisting fibrous structure (Fig. 1(D)). The HRTEM image of PI/CNTs (Fig. 1(B)) exhibits slightly larger diameters and a wavier surface, compared to the CNTs, suggesting the PI coating on the external surface of CNTs. Based on the SEM images in Fig. 1(D) and Fig. 1(E), the PI/CNTs have similar morphology and size to

the CNTs, indicating a thin coating of PI on CNTs. However, the PI sample displays large aggregates (Fig. 1(C) and (F)). The element distribution of CNTs and PI/CNTs (22%) was studied by EDX elemental mapping. By comparing the distributions of elements C, N and O of CNTs (Fig. 1(H), Fig. 1(I), (Fig. 1(J)) and PI/CNTs (22%) (Fig. 1(L), Fig. 1(M), Fig. 1(N)), the presence of N and O is clearly seen throughout the nanotube for the PI/CNTs sample while almost none of N and O is shown on the CNTs. N and O appear uniform in the EDX elemental mapping of PI/CNTs (Fig. 1(M) and Fig. 1(N)). Particularly, the N mapping in Fig. 1(M) is generated from the PI, which clearly indicates the formation of PI on the CNTs for the PI/CNTs sample.

The crystallinity of PI, CNTs and PI/CNTs (22%) samples was studied by PXRD analysis. As indicated in Fig. S2, the pure PI presents significant characteristic peaks in the range of 10-30°, where the intense peak at 29.6° is for the typical graphite interlayer (~ 0.300 nm) [28]. The high crystallinity of pure PI demonstrates high regularity of polymer chains, which is attributed to the strong π–π interactions between conjugated cores during the imidization reaction. However, the typical pattern of PI is not shown in the PI/CNTs (22%) composite, which is likely due to the low loading of PI on the surface of CNTs, consistent with the observation in HRTEM and EDX elemental mapping. Similar results have been found in other studies [25,29].

The FT-IR spectra of CNTs, PI and PI/CNTs (22%) samples were studied to further investigate the composition of the materials (Fig. 2(A)). The two bands at 1771 cm^{-1} and 1723 cm^{-1} are respectively assigned to the asymmetric stretching and symmetric

stretching of C=O [30]. The band around 1300 cm^{-1} is assigned to the stretching vibration of C-N-C in the five-membered imide rings [20]. The band described above can be seen clearly in the pure PI, but is absent from the spectrum of the pure CNTs. The spectrum of PI/CNTs shows a distinct absorption peak of C=O and a larger peak of C-N-C than the pure CNTs, indicating the presence of PI on the CNTs.

N_2 adsorption-desorption isotherms of PI, PI/CNTs (22%) and CNTs are shown in Fig. 2(B). The CNTs and PI/CNTs (22%) samples show the feature of typical IV sorption isotherms with hysteresis loops, indicating that the mesopores exist in the materials and the type of pore structure is not changed after loading the PI onto CNTs. The distinct decrease of specific surface area from 127 to 85 m^2/g further demonstrates the loading of PI on the CNTs. The pure PI sample has a surface area of only 4 m^2/g, which is much smaller than PI/CNTs (22%).

The coordination and nature of the carbon, nitrogen, and oxygen in the CNTs and PI/CNTs (22%) were evaluated and compared by XPS analysis (Fig. 2(C-F)). The survey XPS spectrum of PI/CNTs (22%) shows stronger signals of C, N and O elements, while no obvious signals of N element are observed in the XPS spectrum of the CNTs (Fig. 2(C)). The C1s spectra of CNTs and PI/CNTs almost overlap with each other except that there is a small peak around 289 eV and a visible shoulder at about 287 eV (Fig. 2(D)), which can be attributed to the C=O group and C-O group, respectively, based on the peak deconvolution (Table S1 and Fig. S3(A)) [31]. There is a strong N1s signal from PI/CNTs whilst no peak is shown from the CNTs sample (Fig 2(E)),

indicating the successful formation of PI on CNTs. It looks there are two peaks for the N1s spectrum of the PI/CNTs sample. The peak fitting process shows three deconvoluted peaks but with one peak (C-N-H) much smaller than the other two peaks ($N-(C)_3$ and C=N-C) (Fig. S3(B) and Table S1) [32]. Both O1s peaks from the CNTs and PI/CNTs samples are broad, suggesting multiple species in the samples (Fig. 2(F)) [33].

3.2. Degradation of organic pollutants with PMS

The performance of the PI/CNTs catalyst on PMS activation and degradation of organic contaminants was evaluated by using AO7 as a model pollutant. As shown in Fig. 3(A), the presence of only PMS or PI/CNTs can hardly degrade AO7. Although it was reported in previous research that PI could activate PMS to degrade the contaminant in the wastewater under visible light irradiation [30], it was not observed in this study. Effective activation of PMS and degradation of AO7 at room temperature were not observed when only PI or CNTs or the physical mixture of PI and CNTs were used in the presence of the PMS, all of which produced less than 9.8% removal rate in 20 min. However, after PI was loaded on CNTs, PI/CNTs showed high degradation efficiency with a removal rate of 98% in 15 min in the presence of PMS at room temperature without the light irradiation, suggesting that the loading of PI on CNTs can efficiently activate PMS and degrade the organic pollutant. The error bars for the degradation of AO7 with PI/CNTs + PMS were in the range of 0.1% - 4.2%, confirming good reproducibility and high performance of this new catalyst.

In addition to AO7, the degradations of other organic dyes including MB, X-3B, KN-R, MO and RhB (the structures of these dyes are given in Fig. S4) were examined using the PI/CNTs (22%) catalyst. It was found that all these organic dyes in water could be degraded efficiently by PI/CNTs (22%) with PMS (Fig. 3(B)). These findings demonstrate that PI/CNTs (22%) can efficiently activate the PMS for degradation of a range of organic pollutants.

The effect of light irradiation was further investigated on the PMS activation with PI/CNTs using the AO7 solution, where the degradation reactions were performed under four conditions: in the dark, indoor, exposed under sunlight, and exposed under visible light. As shown in Fig. 3 (C), the removal rate of AO7 is 73% in the dark within 7.5 min and increases significantly in the presence of the light irradiation. When the sunlight and visible light are used as the light irradiation source, AO7 can be completely degraded within 7.5 min. However, it is clear that the degradation of AO7 is still highly efficient with the indoor light condition (without sunlight or visible light). The rest of the experiments in this study were performed without light irradiation, i.e., with normal indoor light.

Because PI is the active component in the PI/CNTs catalysts, the loading of PI was thus investigated. It was noticed that the catalytic capability of the PI/CNTs was strongly correlated with the loading content of PI precursor in the reaction mixture. As seen in Fig. 3(D), the degradation rate of AO7 is initially increased and then decreased with the increased PI loading in the PI/CNTs catalysts. A highest AO7 degradation

efficiency is achieved with the PI/CNTs (22%). This may be explained by the status and amount of PI particles on CNTs. At low PI loading content, PI is uniformly distributed with high exposed surface area and better attachment to the CNTs, resulting in higher catalytic efficiency. The increased loading of PI, and hence the increased active sites, improves the catalytic efficiency of PI/CNTs. However, when the PI loading content is increased further, large PI aggregates are formed, leading to low surface area, poor adhesion of PI on CNTs, and therefore low catalytic efficiency.

3.3. Effects of reaction parameters

Further experiments were conducted to investigate the effects of reaction conditions on degradation rate of AO7 by PMS using the PI/CNTs (22%) as a catalyst. As indicated in Fig. 4(A), the amount of catalyst is varied in order to investigate its effect on degradation of AO7. Enhanced AO7 degradation rates are observed when increasing the PI/CNTs concentration from 0.04 g/L to 0.2 g/L. 43% removal rate of the pollutant AO7 is achieved within 30 min using 0.04 g/L PI/CNTs, while the same degradation rate can be attained within 5, 2.5 and 1 min at the PI/CNTs amount of 0.06, 0.1, and 0.2 g/L in the reactions, respectively. The results can be attributed to the increased concentration of active sites after adding more catalyst and generating more reactive radicals by activating PMS.

The influence of PMS concentration on the degradation rate of AO7 is shown in Fig. 4(B). AO7 is slowly decomposed with a removal percentage of 25% after 20 min in the presence of 0.05 g/L PMS. This incomplete degradation of AO7 can be attributed

to the lack of oxidant species. Under the same conditions, when PMS concentration is increased to 0.1 g/L, the degradation rate of the dye is increased to nearly 66%. At PMS concentration of 0.5 g/L, almost 100% of AO7 is degraded within 7.5 min. The increasing degradation rate of AO7 is resulted from more active radicals generated at higher PMS concentrations. While keeping the PMS concentration constant at 0.1 g/L, the initial concentrations of AO7 were varied (Fig. 4(C)). It can be seen that the degradation efficiency decreases with increasing AO7 concentration. This can be reasoned that at higher concentrations of AO7, more catalysts/active sites would be required for the reaction, leading to lower efficiency in dye degradation.

The effect of reaction temperature on the degradation of AO7 is illustrated in Fig.4(D). The degradation rate significantly increases with the increase of reaction temperature. When the temperature is at 35^{o}C, the dye has almost completely degraded within 7.5 min, while just 42% degradation is achieved at a temperature of 5 ^{o}C.

The effect of initial solution pH on the catalytic performance of PI/CNTs/PMS system was also studied at six different pH values. As indicated in Fig. 4(E), the degradation rate of AO7 is decreased as the pH value is reduced from 9.1 to 2.6. In alkaline medium, the dye can be almost completely degraded within 3 min. The degradation rate becomes slower under weak acid medium condition with an initial pH of 6.3 and 4.9, although 100% removal rate of AO7 is still achieved within 5 min. High degradation efficiency is believed to be associated with the number of active radicals, which are a result of the decomposition of PMS. The relatively higher stability of the

oxidant at acidic pH reduces the generation of radicals, leading to a smaller number of radicals and lower degradation of AO7. In addition, under acidic conditions, the formation of H-bond between H^+ and the O-O group of HSO_5^- would be more significant, which could reduce the negative charge of HSO_5^- and hinder the interaction between HSO_5^- and the catalyst surface [34]. Furthermore, the production of $^1O_2$ for dyes in aerated solutions is approximately five times more efficient in basic medium than in acidic medium [35]. When the catalytic reaction is carried out in the acidic medium below pH 3.5, a much slower degradation rate of AO7 is observed. However, a degradation efficiency of 92% is still observed within 15 min at pH 2.6, suggesting that the as-prepared PI/CNTs metal-free catalyst exhibits good catalytic activities under a broad range of pH values.

3.4. Comparison with other catalysts

The PI/CNTs catalyst was compared to other catalysts for the degradation of AO7 and RhB with PMS. As shown in Table 1, 98% of AO7 could be degraded within 15 min with 0.1g/L catalyst, which is similar to other catalysts such as the nanocomposites of ordered mesoporous silica & CNTs [36] and Co-doped activated carbon [37] (both cases using larger amounts of catalysts). In addition, the PI/CNTs catalyst shows similar or better RhB degradation efficiency compared with metal and other metal-free catalysts, such as Mn_3O_4/ZIF-8[38], h-BN/g-C_3N_4[29] and Fe_3O_4@C/PB[39]. These results suggest that the PI/CNTs catalyst exhibits excellent degradation efficiency for both AO7 and RhB with the PMS system.

3.5. Analysis of intermediate products

The variation in optical absorption spectra during the AO7 reaction under the PI/CNTs/PMS system is given in Fig. 5. While the distinctly decreased absorption intensity at 484 nm indicates the decomposition of the dye's chromophoric structure in the vicinity of the azo-linkage, the reduction at 230 nm shows the destruction of the benzene ring. Besides, the absorbance at 254 nm increases during the initial 15 min and then decreases (Fig. 5 inset), likely due to the production and further decomposition of naphthalene type products[40-42]. These intermediates can be further determined with ESI (Fig.6). There are small peaks of m/z 373 and m/z 327 corresponding to [AO7 + $Na]^+$ and [AO7 - $Na]^-$ after five minutes. Aromatic intermediates such as p-phenolsulfonic acid (m/z 173) and 1,2-naphthaquinone (m/z 181) can be identified as the N=N cleavage of the AO7, which are further hydroxylated by the radicals [30]. The degradation mechanism of AO7 with the PI/CNTs/PMS system is proposed in Fig.S5. Under the visible light irradiation, the reaction rate of the degradation becomes faster. This can be confirmed by comparing the absorbance at the reaction time of 7.5 min with and without visible light irradiation (Fig. S6 and Fig. 3(C)). However, the intermediates determined in the reaction solution under the visible light irradiation are similar to those in the dark.

3.6. Recyclability of the catalyst

Cost evaluation for the preparation and processing of the catalysts and reactions (including chemicals, solvents, electricity) is important for newly developed

technologies. The costs of this study are evaluated against some other studies which also use carbon nanotubes for dye degradation (Table S2). The cost looks reasonable, particularly because high initial concentration and low final concentration are observed in the reactions. The cost may be further reduced by recycling the catalyst. As such, the stability and recyclability of the metal-free catalyst PI/CNTs were evaluated. The degradation reaction could be re-initiated by adding the PI/CNTs (collected from the last reaction) into a fresh solution. As shown in Fig.7, the degradation rate of AO7 is up to 98% within 15 min during the first reaction; 92% of AO7 is degraded within a longer time (35 min) for the second reaction. The efficiency has reduced slowly with the increasing recycling number of the catalyst. It is likely due to the decrease in adsorption sites of the PI/CNTs, as the surface area was found to decrease from 85 m^2/g to 75 m^2/g. After the recycling test with four reactions, the filtered PI/CNTs catalyst was analyzed by PXRD and FT-IR, with the data given in Fig.S7 and Fig.S8. The diffraction intensity of the used PI/CNTs is similar to the fresh catalyst in the PXRD spectra. In the FT-IR spectra, the used PI/CNTs do not present distinct structural changes comparing to the fresh catalyst. The results demonstrate the good stability of the PI/CNTs in the reaction system.

3.7. Investigation of reactive species and mechanism

Sulfate and hydroxyl radicals could be generated during PMS activation by metal-free or metal-based catalysts [43,44]. In this work, EPR was used to experimentally probe the presence of radicals using DMPO as a radical spin trapping agent. As

indicated in Fig. 8(A), no noticeable signals are observed in the system for PI or CNTs with PMS. However, in the PI/CNTs/PMS system, a signal pattern indicating the formation of DMPOX via direct oxidation of DMPO through non-radical pathway is shown whilst the characteristic peaks of DMPO-OH and DMPO-SO_4 adducts do not appear [45-47]. Competitive quenching tests were conducted to determine the existence of different radicals. The rate constants of quenching reaction of HO• and SO_4^-• radicals and $^1O_2$ by scavengers are given in Table S3. Ethanol and tert-butanol can quench the reaction of HO• and SO_4^-• radicals easily. To further verify the effects of HO• and SO_4^-• radicals on the degradation of AO7, quenching tests were conducted with ethanol and tert-butanol as the scavengers in this study. For our catalyst system, after adding ethanol and tert-butanol into the reaction or performing the reaction in ethanol, little effect on AO7 degradation during PMS activation is observed (Fig. 8(B)). These results indicate that HO• and SO_4^-• radicals are not mainly responsible for the degradation of AO7 [48].

It has been demonstrated that $^1O_2$ could be produced during the self-decomposition of PMS [49], by the reaction based on Eq (1), where the generation of $^1O_2$ was facilitated by ketones and carbonaceous materials during PMS activation [50].

$$HSO_5^- + SO_5^{2-} \rightarrow HSO_4^- + SO_4^{2-} + {}^1O_2 \quad (1)$$

TMP is usually used to trap $^1O_2$ and the product can be detected as a three-line peak with equal intensity in the EPR spectrum. It should be noted that TMP cannot be oxidized when used alone (i.e., without $^1O_2$) and as a result the typical three-line peaks in EPR spectrum would not be produced [43,51]. For the work in our study, as shown

in Fig. 9(A), the typical patterns of three-line peaks for TMP-$^1O_2$ are observed in the EPR spectra for all the samples after adding TMP, including PMS, CNTs/PMS, PI/PMS, and PI/CNTs/PMS systems. The intensity of the peaks in the PI/CNTs/PMS system is much stronger than the other systems, indicating more $^1O_2$ has been generated during the PMS activation with the PI/CNTs catalyst. Furthermore, the continuous generation of singlet oxygen with increasing peak intensity can be seen in the PI/CNTs /PMS system for the 10 min reaction (Fig. 9(B)). It can be deduced that $^1O_2$ plays a dominant role in the degradation of AO7 by activating PMS. NaN_3 can quench both HO• and SO_4^- • radicals and also $^1O_2$, while ethanol and tert-butanol are effective scavengers only for HO• and SO_4^-• radicals (Table S3). Quenching tests were thus conducted to verify the presence of $^1O_2$ using NaN_3 as the scavenger. As shown in Fig.10, the degradation efficiency of AO7 is considerably hindered when NaN_3 is added into the PI/CNTs/PMS system. The degradation rate of AO7 decreases as the concentration of NaN_3 in the solution increases. Compared with the slight inhibitory effects of ethanol and tert-butanol on AO7 degradation (Fig. 8(B)), the significant impact of adding NaN_3 on the degradation of AO7 indicates that $^1O_2$ is the main contributor to AO7 degradation in the PI/CNTs /PMS system.

Singlet-oxygen chemiluminescence measurements have been performed to evaluate whether the recombination of superoxide radicals ($\cdot O_2^-$) exists during the formation of $^1O_2$. The superoxide radicals are generated as an intermediate in the presence of the dissolved oxygen [52,53]. Superoxide radicals produced during the

reaction can be subsequently recombined to form $^1O_2$ (Eq(2)).

$$2 \cdot O_2^- + 2H_2O \rightarrow {}^1O_2 + H_2O_2 + 2OH^- \quad (2)$$

In order to prove whether $\cdot O_2^-$ was generated in the PI/CNTs/PMS system, benzoquinone (BQ) was added as the quenching agent. As seen in Fig. S9, the degradation efficiency of AO7 is clearly decreased with the increasing concentration of BQ added into the reaction. The results demonstrate that $\cdot O_2^-$ is generated in the process of the PI/CNTs/PMS reaction system.

For aqueous solutions with generated singlet oxygen, it has been found that the concentration of dissolved oxygen (DO) could increase because singlet oxygen could decay rapidly to triplet oxygen ($^3O_2$), which could provide evidence for the existence of $^1O_2$ [5,52]. Therefore, the concentration of DO in our reactions was measured. Higher DO concentration or rapid increase in DO concentration were observed when PI/CNTs + PMS were added into the solution (Fig. S10), suggesting the generation of singlet oxygen during the reaction.

Based on the above experimental results, it can be claimed that $^1O_2$, instead of hydroxyl radical (HO•) and sulfate radical (SO_4^-•), plays a dominant role during the catalytic oxidation of AO7 in the PI/CNTs/PMS system. The possible reaction mechanism for AO7 degradation in the PI/CNTs/PMS system is similar to the non-radical mechanism proposed for CNTs in the literature [18].

It has been reported that the introduction of heteroatoms into the graphene layer

could disrupt sp^2-hybridized carbon configuration and modulate the physical, chemical, and electrical properties of graphene, creating new active sites for various reactions[33]. Theoretical studies indicated that the graphitic N, with a smaller covalent radius and higher electronegativity than the C atom, could induce electron transfer from adjacent carbon atoms to nitrogen, thus breaking the chemical inertness of the sp^2 carbon layer and altering the catalytic activity of graphene[42]. Carbonyl groups like C=O at the boundaries of carbonaceous materials were proposed to be the crucial chemical reactive sites in the activation of PMS [54]. PI molecules possess abundant electronegative N (C-N and C=N-C) and C=O groups. Thus, the loading of PI on the surface of CNTs makes PI/CNTs possess abundant chemical reactive sites at the boundaries of CNTs. In addition, the enhanced adsorption of pollutants and PMS caused by electronegative N atoms and the positively polarized carbon atoms on the surface of PI/CNTs can facilitate the contact of the pollutants with the reactive oxidized species generated from the activation of PMS, and further improve the catalytic performance. It is found that the efficiency of AO7 degradation is significantly improved from 2.2% to 98.9% within 15min when the catalyst is changed from pure PI to PI/CNTs (22%) in the PMS system (Fig. 2), indicating that electronegative N and C=O groups at the defective edges of PI/CNTs may play an important role in the redox process for PMS activation as expected.

4. Conclusion

In summary, polyimide-modified CNTs (PI/CNTs) catalysts were synthesized

through an *in situ* thermal method. The catalytic ability of the PI/CNTs materials was strongly correlated with the loading of PI in the reaction mixture. The as-prepared PI/CNTs (22%) showed a high performance for organic pollutant degradation by activating PMS without light irradiation. The degradation efficiency of AO7 was significantly enhanced to 98.9% within 15 min, compared to 2.2% produced by using pure PI. The as-prepared PI/CNTs catalysts also displayed good stability. The investigation into reactive species of the PI/CNTs/PMS system showed that singlet oxygen ($^1O_2$), instead of hydroxyl radical (HO•) or sulfate radical (SO_4^-•), played the dominant role in the efficient degradation of organic pollutants. As an environmental-friendly metal-free catalyst, PI/CNTs has shown very good potential for activating PMS to degrade organic pollutants in water.

Acknowledgement

MW acknowledges the joint Ph.D studentship from China Scholarship Council for the financial support. Useful suggestions given by Liang Zeng, Gang Nie and Longlong Zhu of Wuhan University are also acknowledged.

References

[1] E. Bloem, A. Albihn, J. Elving, L. Hermann, L. Lehmann, M. Sarvi, T. Schaaf, J. Schick, E. Turtola, K. Ylivainio, Contamination of organic nutrient sources with potentially toxic elements, antibiotics and pathogen microorganisms in relation to P fertilizer potential and treatment options for the production of sustainable fertilizers: A review, Sci. Total Environ. 607–608 (2017) 225–242.

[2] H. Wei, W. A. McMaster, J. Z. Y. Tan, D. Chen, R. A. Caruso, Tricomponent brookite/anatase TiO_2/g-C_3N_4 heterojunction in mesoporous hollow microspheres for enhanced visible-light photocatalysis, J. Mater. Chem. A. 6 (2018) 7236–7245.

[3] A. Manivel, G. J. Lee, C. Y. Chen, J. H. Chen, S. H. Ma, T. L. Horng, J. J. Wu, Synthesis of MoO_3 nanoparticles for azo dye degradation by catalytic ozonation, Mater. Res. Bull. 62 (2015) 184–191.

[4] V. S. Antonin, S. Garcia-Segura, M. C. Santos, E. Brillas, Degradation of Evans Blue diazo dye by electrochemical processes based on Fenton's reaction chemistry, J. Electroanal. Chem. 747 (2015) 1–11.

[5] Y. Liu, H. Guo, Y. Zhang, W. Tang, X. Cheng, W. Li, Heterogeneous activation of peroxymonosulfate by sillenite $Bi_{25}FeO_{40}$: Singlet oxygen generation and degradation for aquatic levofloxacin, Chem. Eng. J. 343 (2018) 128–137.

[6] M. Wei, Y. Ruan, S. Luo, X. Li, A. Xu, P. Zhang, The facile synthesis of a

magnetic OMS-2 catalyst for decomposition of organic dyes in aqueous solution with peroxymonosulfate, New J. Chem. 39 (2015) 6395–6403.

[7] X. Duan, C. Su, J. Miao, Y. Zhong, Z. Shao, S. Wang, H. Sun, Insights into perovskite-catalyzed peroxymonosulfate activation: Maneuverable cobalt sites for promoted evolution of sulfate radicals, Appl. Catal. B Environ. 220 (2018) 626–634.

[8] S. Norzaee, M. Taghavi, B. Djahed, F. Kord Mostafapour, Degradation of Penicillin G by heat activated persulfate in aqueous solution, J. Environ. Manage. 215 (2018) 316–323.

[9] M. Wei, L. Gao, J. Li, J. Fang, W. Cai, X. Li, A. Xu, Activation of peroxymonosulfate by graphitic carbon nitride loaded on activated carbon for organic pollutants degradation, J. Hazard. Mater. 316 (2016) 60–68.

[10] D. Zhou, L. Chen, J. Li, F. Wu, Transition metal catalyzed sulfite auto-oxidation systems for oxidative decontamination in waters: A state-of-the-art minireview, Chem. Eng. J. 346 (2018) 726–738.

[11] X. Shi, X. Chen, X. Chen, S. Zhou, S. Lou, Y. Wang, L. Yuan, PVP assisted hydrothermal synthesis of BiOBr hierarchical nanostructures and high photocatalytic capacity, Chem. Eng. J. 222 (2013) 120-127.

[12] J. Lu, J. Wu, Y. Ji, D. Kong, Transformation of bromide in thermo activated persulfate oxidation processes, Water Res. 78 (2015) 1–8.

[13] S. Verma, S. Nakamura, M. Sillanpää, Application of UV–C LED activated PMS for the degradation of anatoxin-a, Chem. Eng. J. 284 (2016) 122–129.

[14] G. P. Anipsitakis, D. D. Dionysiou, Radical generation by the interaction of transition metals with common oxidants radical generation by the interaction of transition metals with common oxidants, Environ. Sci. Technol. 38 (2004) 3705–3712.

[15] G. P. Anipsitakis, D. D. Dionysiou, Transition metal/UV-based advanced oxidation technologies for water decontamination, Appl. Catal. B Environ. 54 (2004) 155–163.

[16] S. Xavier, R. Gandhimathi, P. V. Nidheesh, S. T. Ramesh, Comparison of homogeneous and heterogeneous Fenton processes for the removal of reactive dye Magenta MB from aqueous solution, Desalin. Water Treat. 53 (2013) 109–118.

[17] H. Sun, C.K. Kwan, A. Suvorova, H. M. Ang, M. O. Tadé, S. Wang, Catalytic oxidation of organic pollutants on pristine and surface nitrogen-modified carbon nanotubes with sulfate radicals, Appl. Catal. B Environ. 154–155 (2014) 134–141.

[18] H. Lee, H. J. Lee, J. Jeong, J. Lee, N. B. Park, C. Lee, Activation of persulfates by carbon nanotubes: Oxidation of organic compounds by nonradical mechanism, Chem. Eng. J. 266 (2015) 28–33.

[19] W. Ma, N. Wang, Y. Fan, T. Tong, X. Han, Y. Du, Non-radical-dominated catalytic degradation of bisphenol A by ZIF-67 derived nitrogen-doped carbon nanotubes frameworks in the presence of peroxymonosulfate, Chem. Eng. J. 336 (2018) 721–731.

[20] M. Zhang, H. Niu, D. Wu, Polyimide fibers with high strength and high modulus: preparation, structures, properties, and applications, Macromol. Rapid Commun. 39 (2018) 1800141.

[21] H. Ni, J. Liu, Z. Wang, S. Yang. A review on colorless and optically transparent polyimide films: Chemistry, process and engineering applications, J. Ind. Eng. Chem. 28 (2015) 16-27.

[22] S. Chu, Y. Wang, Y. Guo, P. Zhou, H. Yu, L. Luo, F. Kong, Z. Zou, Facile green synthesis of crystalline polyimide photocatalyst for hydrogen generation from water, J. Mater. Chem. 22 (2012) 15519–15521.

[23] Y. Guo, S. Chu, S. Yan, Y. Wang, Z. Zou, Developing a polymeric semiconductor photocatalyst with visible light response, Chem. Commun. 46 (2010) 7325–7327.

[24] T. Yan, M. Li, X. Wang, M. Sun, H. Liu, Q. Wei, W. Xu, B. Du, Facile preparation of novel organic–inorganic PI/$Zn_{0.25}Cd_{0.75}S$ composite for enhanced visible light photocatalytic performance, Appl. Surf. Sci. 340 (2015) 102–112.

[25] J. Y. Li, X. Jiang, L. Lin, J. J. Zhou, G. S. Xu, Y. P. Yuan, Improving the photocatalytic performance of polyimide by constructing an inorganic-organic

hybrid ZnO-polyimide core-shell structure, J. Mol. Catal. A Chem. 406 (2015) 46–50.

[26] C. Wang, Y. Guo, Y. Yang, S. Chu, C. Zhou, Y. Wang, Z. Zou, Sulfur-doped polyimide photocatalyst with enhanced photocatalytic activity under visible light irradiation, ACS Appl. Mater. Interfaces. 6 (2014) 4321–4328.

[27] S. Chu, Y. Wang, Y. Guo, J. Feng, C. Wang, W. Luo, X. Fan, Z. Zou, Band structure engineering of carbon nitride: In search of a polymer photocatalyst with high photooxidation property, ACS Catal. 3 (2013) 912–919.

[28] Z. Xu, X. Zhuang, C. Yang, J. Cao, Z. Yao, Y. Tang, J. Jiang, D. Wu, X. Feng, Nitrogen-doped porous carbon superstructures derived from hierarchical assembly of polyimide nanosheets, Adv. Mater. 28 (2016) 1981–1987.

[29] L. Jiang, X. Yuan, G. Zeng, Z. Wu, J. Liang, X. Chen, L. Leng, H. Wang, H. Wang, Metal-free efficient photocatalyst for stable visible-light photocatalytic degradation of refractory pollutant, Appl. Catal. B Environ. 221 (2018) 715–725.

[30] Y. Tao, M. Wei, D. Xia, A. Xu, X. Li, Polyimides as metal-free catalysts for organic dye degradation in the presence peroxymonosulfate under visible light irradiation, RSC Adv. 5 (2015) 98231–98240.

[31] P. Gobbo, M. C. Biesinger, M. S. Workentin, Facile synthesis of gold nanoparticle (AuNP)−carbon nanotube (CNT) hybrids through an interfacial Michael addition reaction. Chem. Commun. 49 (2013) 2831-2833.

[32] S. Naidu Talapaneni, K. Ramadass, S.J. Ruban, M. Benzigar, K. S. Lakhi, J. H. Yang, U. Ravon, K. Albahily, A. Vinu, 3D cubic mesoporous C_3N_4 with tunable pore diameters derived from KIT-6 and their application in base catalyzed Knoevenagel reaction, Catal. Today 324 (2019) 33–38.

[33] X. Cheng, H. Guo, Y. Zhang, Y. Liu, H. Liu, Y. Yang, Oxidation of 2,4-dichlorophenol by non-radical mechanism using persulfate activated by Fe/S modified carbon nanotubes, J. Colloid Interface Sci. 469 (2016) 277–286.

[34] J. Liu, Z. Zhao, P. Shao and F. Cui, Activation of peroxymonosulfate with magnetic Fe_3O_4-MnO_2 core-shell nanocomposites for 4-chlorophenol degradation, Chem. Eng. J. 262 (2015) 854–861.

[35] R. Bonneau, R. Pottier, O. Bagno, J. Joussot, pH dependence of singlet oxygen production in aqueous solutions using thiazine dyes as photosensitizers, Photochem. Photobiol. 21 (1975) 159–163.

[36] M. Wang, Y. Wei, Q. Zou, W. Zhang, A. Xu, X. Li, Tuning manganese (III) species in manganese oxide octahedral molecular sieve by interaction with carbon nanofibers for enhanced pollutant degradation in the presence of peroxymonosulfate, J. Colloid Interface Sci. 536 (2019) 271–280.

[37] T. Huang, J. Chen, Z. Wang, X. Guo, J.C. Crittenden, Excellent performance of cobalt-impregnated activated carbon in peroxymonosulfate activation for acid orange 7 oxidation, Environ. Sci. Pollut. Res. 24 (2017) 9651–9661.

[38] L. Hu, G. Deng, W. Lu, Y. Lu, Y. Zhang, Peroxymonosulfate activation by Mn_3O_4/metal-organic framework for degradation of refractory aqueous organic pollutant rhodamine B, Chinese J. Catal. 38 (2017) 1360–1372.

[39] F. Guo, K. Wang, J. Lu, J. Chen, X. Dong, D. Xia, A. Zhang, Q. Wang, Activation of peroxymonosulfate by magnetic carbon supported Prussian blue nanocomposite for the degradation of organic contaminants with singlet oxygen and superoxide radicals, Chemosphere 218 (2019) 1071–1081.

[40] J. Li, J. Fang, L. Gao, J. Zhang, X. Ruan, A. Xu, X. Li, Graphitic carbon nitride induced activity enhancement of OMS-2 catalyst for pollutants degradation with peroxymonosulfate, Appl. Surf. Sci. 402 (2017) 352–359.

[41] F. Liu, P. Yi, X. Wang, H. Gao, H. Zhang, Degradation of Acid Orange 7 by an ultrasound/ZnO-GAC/persulfate process, Sep. Purif. Technol. 194 (2018) 181–187.

[42] C. Wang, J. Kang, H. Sun, H. M. Ang, M. O. Tadé, S. Wang, One-pot synthesis of N-doped graphene for metal-free advanced oxidation processes, Carbon 102 (2016) 279–287.

[43] C. Guan, J. Jiang, C. Luo, S. Pang, Y. Yang, Z. Wang, J. Ma, J. Yu, X. Zhao, Oxidation of bromophenols by carbon nanotube activated peroxymonosulfate (PMS) and formation of brominated products: Comparison to peroxydisulfate (PDS), Chem. Eng. J. 337 (2018) 40–50.

[44] D. Wu, P. Ye, M. Wang, Y. Wei, X. Li, A. Xu, Cobalt nanoparticles encapsulated in nitrogen-rich carbon nanotubes as efficient catalysts for organic pollutants degradation via sulfite activation, J. Hazard. Mater. 352 (2018) 148–156.

[45] J. Hou, S. Yang, H. Wan, H. Fu, X. Qu, Z. Xu, S. Zheng, Highly effective catalytic peroxymonosulfate activation on N-doped mesoporous carbon for o-phenylphenol degradation, Chemosphere. 197 (2018) 485–493.

[46] L. Wang, J. Jiang, S.Y. Pang, Y. Zhou, J. Li, S. Sun, Y. Gao, C. Jiang, Oxidation of bisphenol A by nonradical activation of peroxymonosulfate in the presence of amorphous manganese dioxide, Chem. Eng. J. 352 (2018) 1004–1013.

[47] J. Li, H. Lin, K. Zhu, H. Zhang, Degradation of Acid Orange 7 using peroxymonosulfate catalyzed by granulated activated carbon and enhanced by electrolysis, Chemosphere 188 (2017) 139–147.

[48] J. Wang, S. Wang, Activation of persulfate (PS) and peroxymonosulfate (PMS) and application for the degradation of emerging contaminants, Chem. Eng. J. 334 (2018) 1502–1517.

[49] P. Liang, C. Zhang, X. Duan, H. Sun, S. Liu, M.O. Tade, S. Wang, An insight into metal organic framework derived N-doped graphene for the oxidative degradation of persistent contaminants: formation mechanism and generation of singlet oxygen from peroxymonosulfate, Environ. Sci. Nano. 4 (2017) 315–324.

[50] D.F. Evans, M.W. Upton, Studies on singlet oxygen in aqueous solution. Part 3.

the decomposition of peroxy-acids, J. Chem. Soc. Dalton Trans. 6 (1985) 1151–1153.

[51] X. Cheng, H. Guo, Y. Zhang, X. Wu, Y. Liu, Non-photochemical production of singlet oxygen via activation of persulfate by carbon nanotubes, Water Res. 113 (2017) 80–88.

[52] Z. Cao, C. Lau, J. Lu, A general chemiluminescence method for the determination of surfactants based on its quenching effect on the luminol-$NaIO_4$-cyclodextrin reaction, Analyst 129 (2004) 1262–1266.

[53] J.M. Lin, M. Yamada, Oxidation reaction between periodate and polyhydroxy compounds and its application to chemiluminescence, Anal. Chem. 71 (1999) 1760–1766.

[54] Z. Zhao, Y. Dai, J. Lin, G. Wang, Highly-ordered mesoporous carbon nitride with ultrahigh surface area and pore volume as a superior dehydrogenation catalyst, Chem. Mater. 26 (2014) 3151–3161.

Table 1

Comparison with other catalysts

Catalyst	Pollutant	Concentration(mg/L)	Dosage(g/L)	Time(min)	Removal(%)	Light source	reference
PI/CNTs	AO7	50	0.1	15	98	No	this study
OC	AO7	50	0.2	20	98	No	[36]
Co-doped AC	AO7	20	0.3	20	97	No	[37]
PI/CNTs	RhB	50	0.1	5	98	No	this study
h-BN/g-C_3N_4	RhB	20	0.5	40	99.5	Yes	[29]
Mn_3O_4/ZIF-8	RhB	10	0.3	40	≈98	No	[38]
Fe_3O_4@C/PB	RhB	10	0.6	40	≈83	No	[39]

AC: activated carbon; OC: OMS (ordered mesoporous silica) and CNTs nanocomposites; h-BN: hexagonal boron nitride; Fe_3O_4@C/PB: magnetic carbon supported Prussian blue nanocomposite

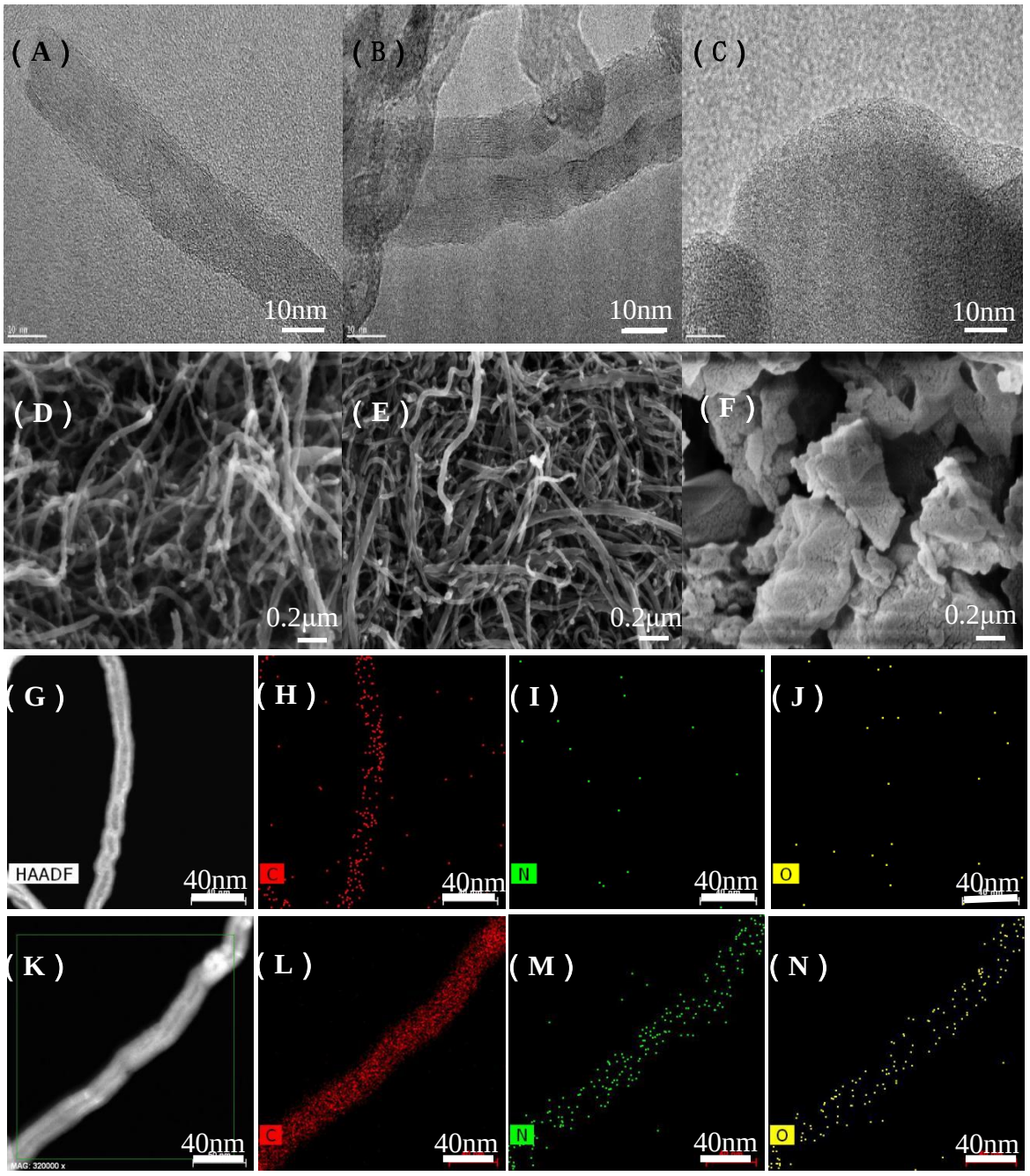

Fig.1. HRTEM images of (A) CNTs, (B) PI/CNTs (22%) and (C)PI, SEM images of (D) CNTs, (E) PI/CNTs (22%) and (F)PI, STEM images of (G) CNT and (K) PI/CNT (22%) and EDX elemental mapping of CNTs ((H), (I), (J)) and PI/CNTs (22%) ((L), (M), (N)) with element C, element N and element O.

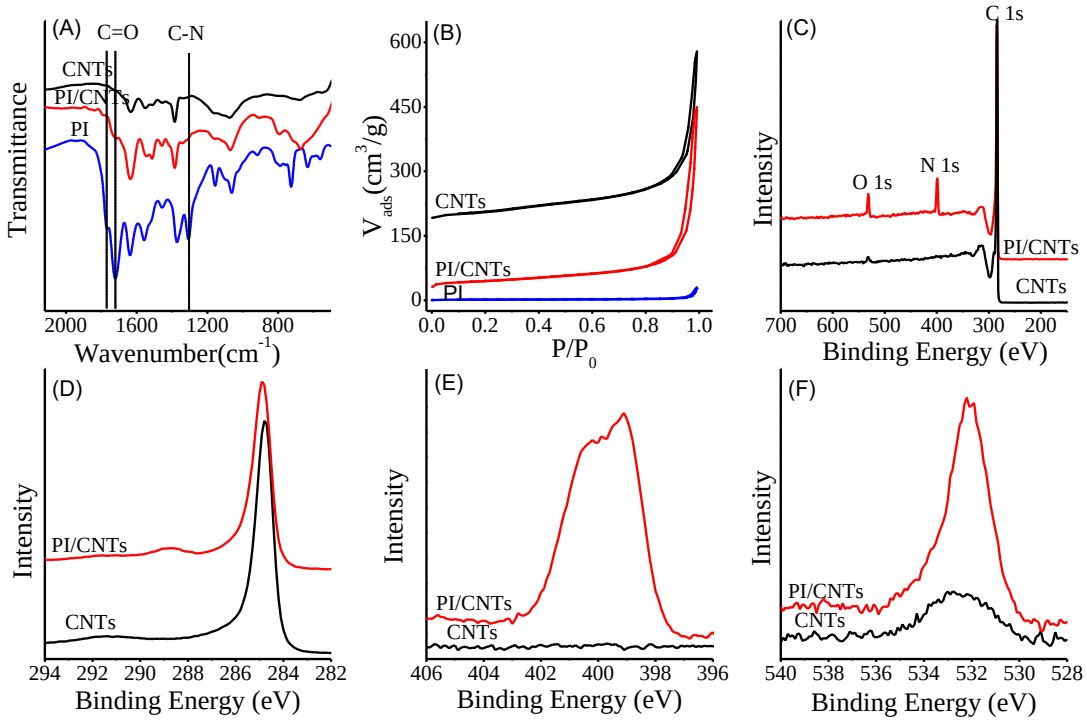

Fig.2. (A) FT-IR spectra and (B) N_2 adsorption isotherms of CNTs, PI/CNTs (22%) and PI. (C) Survey XPS spectra of CNTs and PI/CNTs (22%). (D-F) Comparison of XPS spectra of CNTs and PI/CNTs by C1s (D), N1s (E), and O1s (F).

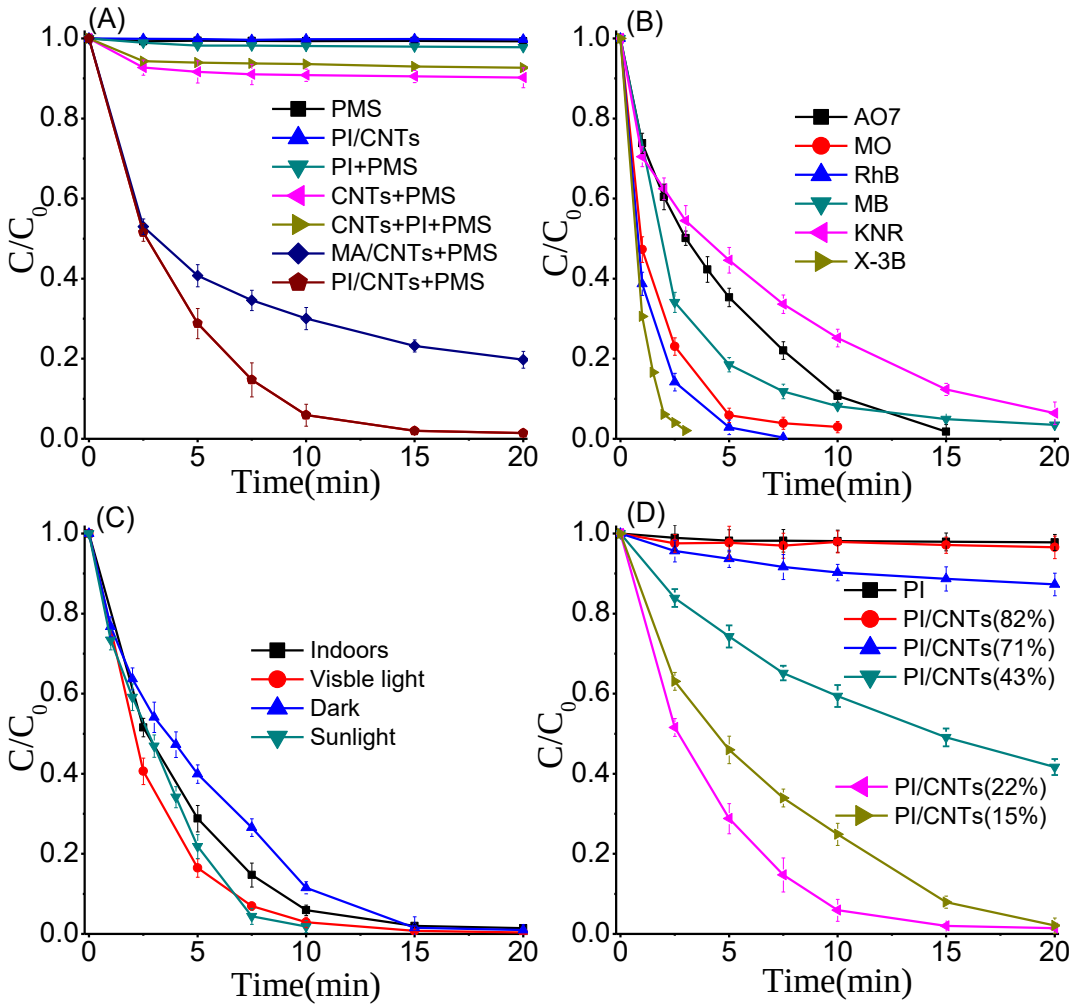

Fig. 3. Degradation of AO7 with PI/CNTs (22%) as the main catalyst. (A) Comparison with other catalysts; (B) Comparison with other dyes; (C) Effect of light irradiation; (D) Effect of PI loading content in the PI/CNTs catalysts. Conditions: PI/CNTs 0.1 g/L, PMS 0.2 g/L, organic pollutants 50 mg/L, 25 ºC.

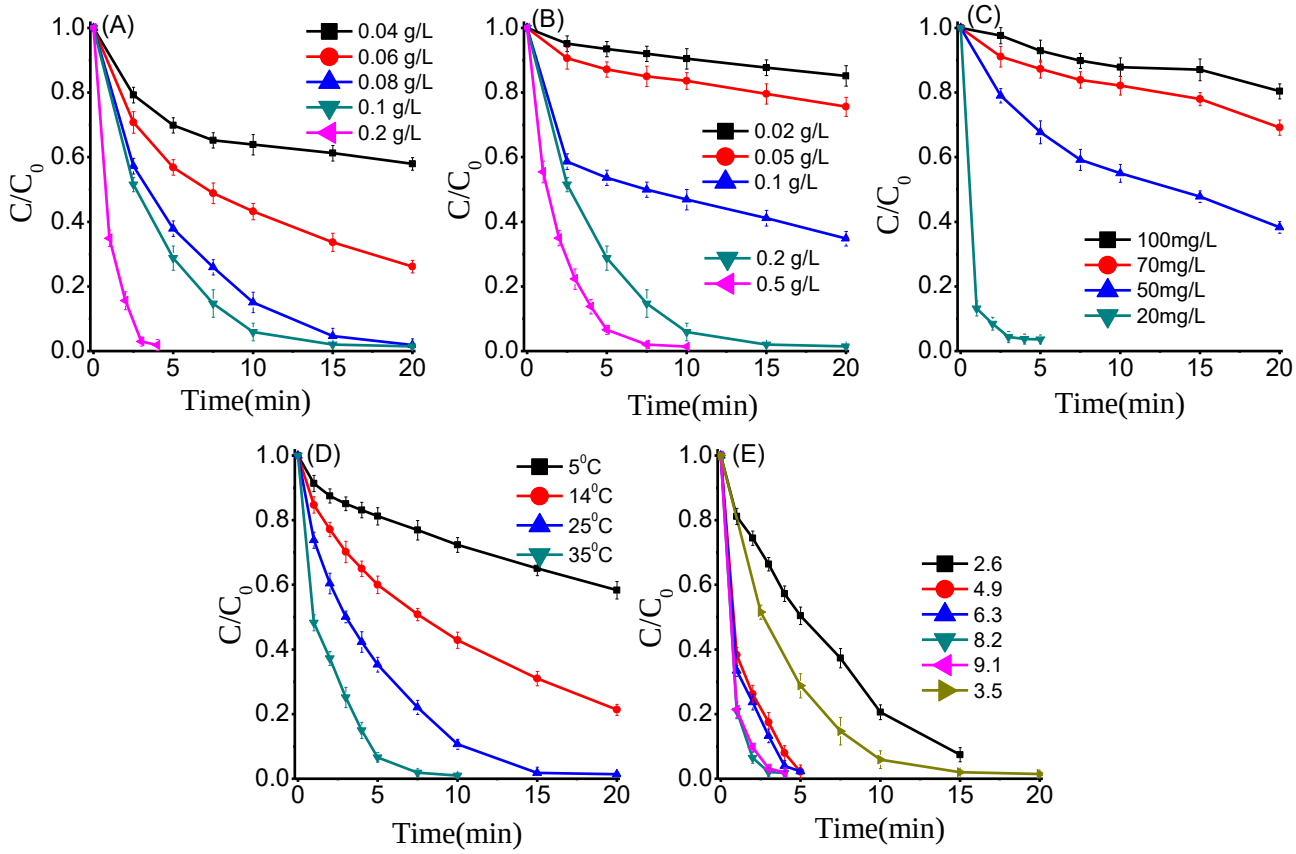

Fig.4. Effects of various parameters on degradation of AO7 using the PI/CNTs (22%)/PMS system. (A) Amount of catalyst; (B) PMS concentrations; (C) AO7 concentrations(PMS 0.1 g/L); (D) Reaction temperature; (E) Solution pH. Standard conditions: PI/CNTs (22%) 0.1 g/L, AO7 50 mg/L, PMS 0.2 g/L, pH 3.5, 25 ^{o}C.

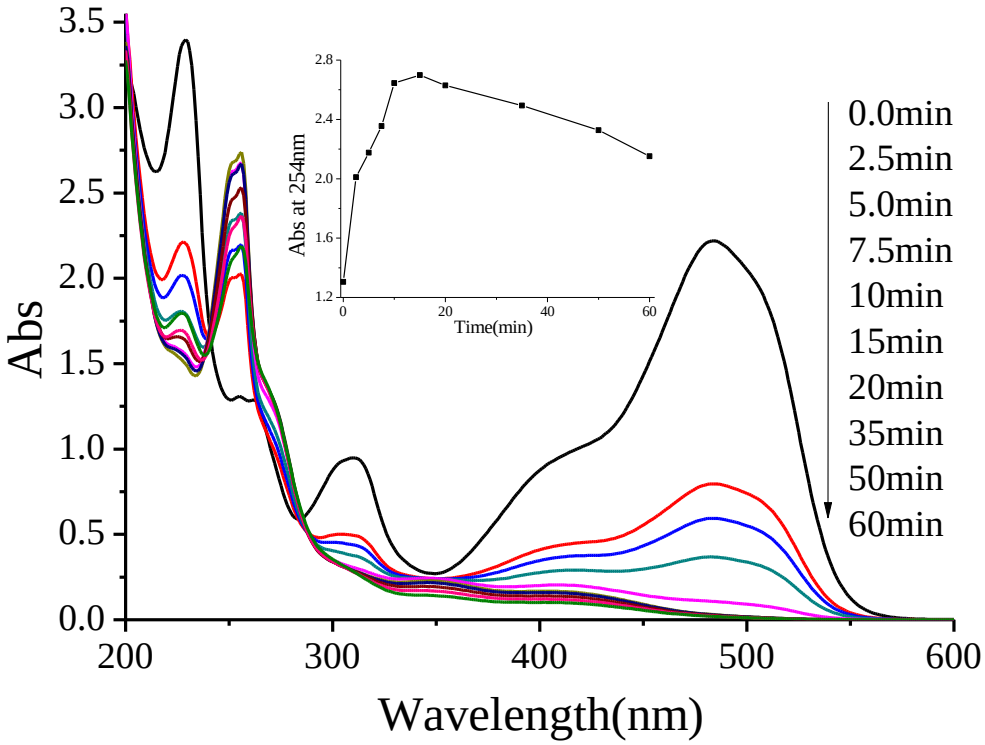

Fig.5. UV-Vis spectra changes during AO7 degradation by PI/CNTs (22%)/PMS system. Conditions: PI/CNTs 0.1 g/L, PMS 0.2 g/L, AO7 50 mg/L, 25 ^{o}C.

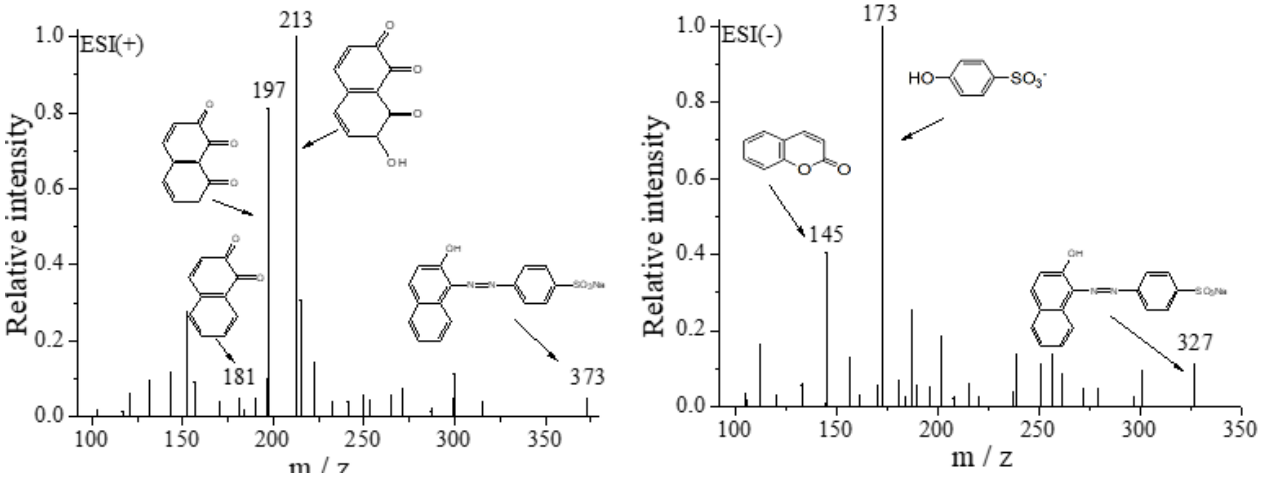

Fig.6. ESI (+) and ESI (-) mass spectra of AO7 solution during the degradation with PI/CNTs (22%)/PMS system in 5min. Conditions: PI/CNTs 0.1 g/L, PMS 0.2 g/L, AO7 50 mg/L, 25 ºC.

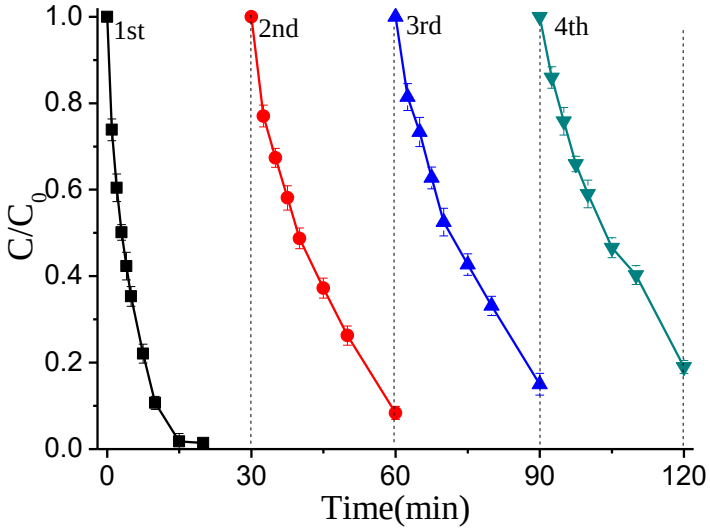

Fig.7. AO7 degradation with the recycled PI/CNTs (22%) catalyst in the presence of PMS. Conditions: PI/CNTs 0.1 g/L, PMS 0.2 g/L, AO7 50 mg/L, 25 ^{o}C.

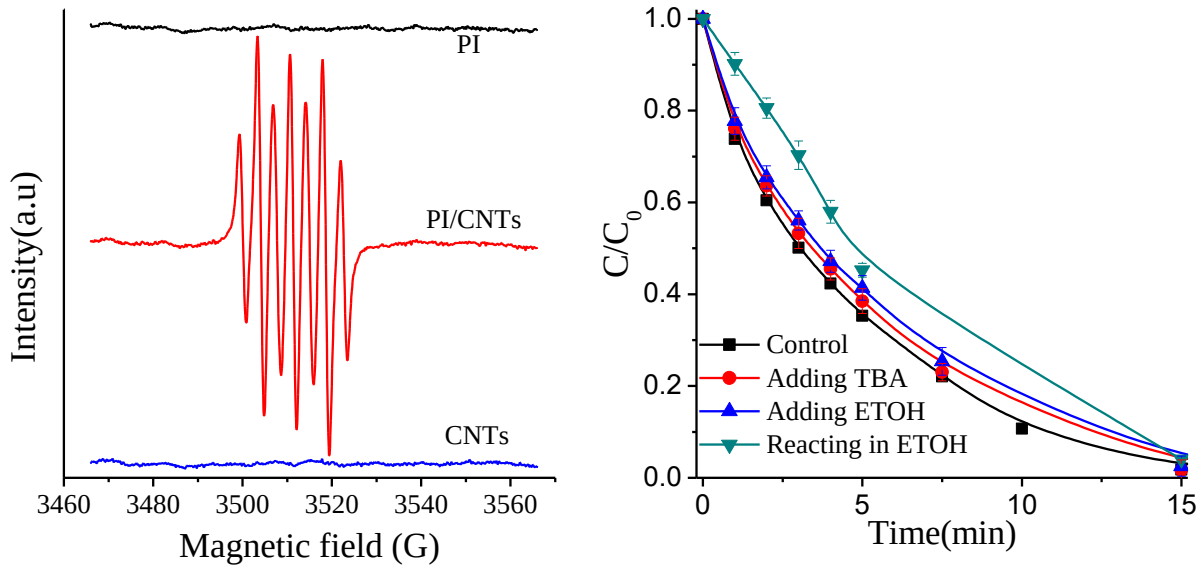

Fig.8. (A)EPR spectra of DMPO-OH and DMPO-SO_4 adducts and (B)Degradation of AO7 by PI/CNTs (22%)/PMS system with the TBA, EtOH. Conditions: PI/CNTs 0.1 g/L, PMS 0.2 g/L, AO7 50 mg/L, DMPO 5mM, reaction time 3min,25 ^{o}C.

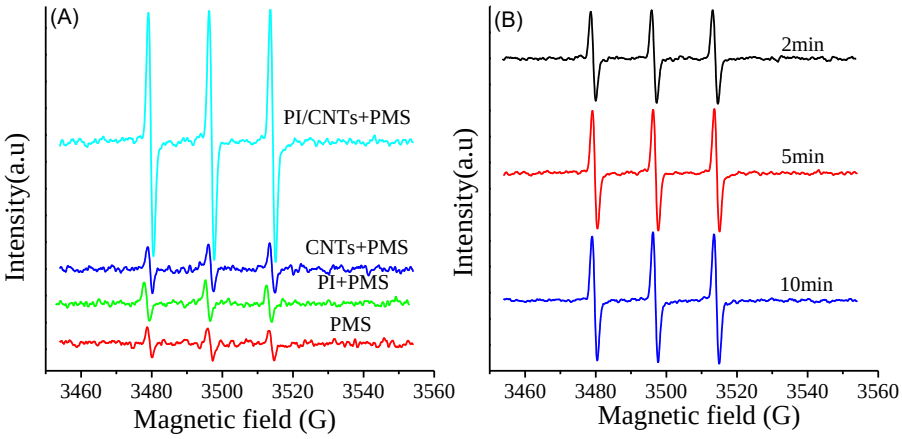

Fig.9. EPR spectra of TMP-$^1O_2$ adducts in different catalytic systems (A) and in the continuous reaction time(B). Conditions: PI/CNTs 0.1 g/L, PMS 0.2 g/L, AO7 50 mg/L, TMP 5mM, 25 ^oC.

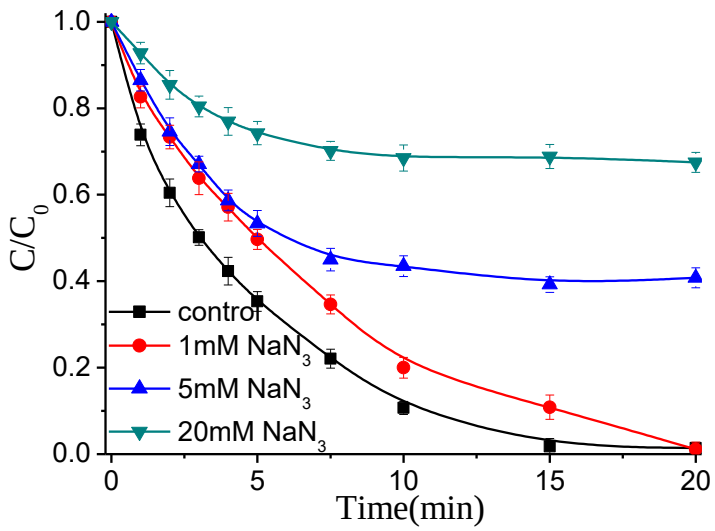

Fig.10. Effect of NaN_3 on decomposition of AO7 in PI/CNTs (22%)/PMS system. Conditions: PI/CNTs 0.1 g/L, PMS 0.2 g/L, AO7 50 mg/L, 25 ^{o}C.